

Contribution of tropical cyclones to atmospheric moisture transport and rainfall over East Asia

Article

Accepted Version

Guo, L., Klingaman, N. P. ORCID: <https://orcid.org/0000-0002-2927-9303>, Vidale, P. L. ORCID: <https://orcid.org/0000-0002-1800-8460>, Turner, A. G. ORCID: <https://orcid.org/0000-0002-0642-6876>, Demory, M.-E. and Cobb, A. (2017) Contribution of tropical cyclones to atmospheric moisture transport and rainfall over East Asia. *Journal of Climate*, 30 (10). pp. 3853-3865. ISSN 1520-0442 doi: 10.1175/JCLI-D-16-0308.1 Available at <https://centaur.reading.ac.uk/68809/>

It is advisable to refer to the publisher's version if you intend to cite from the work. See [Guidance on citing](#).

To link to this article DOI: <http://dx.doi.org/10.1175/JCLI-D-16-0308.1>

Publisher: American Meteorological Society

All outputs in CentAUR are protected by Intellectual Property Rights law, including copyright law. Copyright and IPR is retained by the creators or other copyright holders. Terms and conditions for use of this material are defined in the [End User Agreement](#).

www.reading.ac.uk/centaur

CentAUR

Central Archive at the University of Reading

Reading's research outputs online

1 **Contribution of Tropical Cyclones to atmospheric moisture transport and**
2 **rainfall over East Asia**

3 Liang Guo*

4 *National Centre for Atmospheric Science, Department of Meteorology, University of Reading,*
5 *Reading, United Kingdom*

6 Nicholas P. Klingaman

7 *National Centre for Atmospheric Science, Department of Meteorology, University of Reading,*
8 *Reading, United Kingdom*

9 Pier Luigi Vidale

10 *National Centre for Atmospheric Science, Department of Meteorology, University of Reading,*
11 *Reading, United Kingdom*

12 Andrew G. Turner

13 *National Centre for Atmospheric Science and Department of Meteorology, University of Reading,*
14 *Reading, United Kingdom*

15 Marie-Estelle Demory

16 *National Centre for Atmospheric Science, Department of Meteorology, University of Reading,*
17 *Reading, United Kingdom*

18

Alison Cobb

19

Department of Physics, Imperial College, London, United Kingdom

²⁰ **Corresponding author address:* Department of Meteorology, University of Reading, P.O. Box 243,

²¹ Earley Gate, Reading, UK.

²² E-mail: l.guo@reading.ac.uk

ABSTRACT

23 The coastal region of East Asia (EA) is one of the regions with the most fre-
24 quent impacts from tropical cyclones (TCs). In this study, rainfall and mois-
25 ture transports related to TCs are measured over the EA, and the contribution
26 of TCs to the regional water budget is compared with other contributors, es-
27 pecially the mean circulation of the EA summer monsoon (EASM). Based on
28 ERA-Interim re-analysis (1979–2012), the trajectories of TCs are identified
29 using an objective feature tracking method. Over 60% of TCs occur from
30 July to October (JASO). During JASO, TC rainfall contributes 10-30% the
31 of monthly total rainfall over the coastal region of EA; this contribution is
32 highest over the south/southeast coast of China in September. TCs make a
33 larger contribution to daily extreme rainfall (above the 95th percentile): 50-
34 60% over the EA coast and as high as 70% over Taiwan island. Compared
35 with the mean EASM, TCs transport less moisture over the EA. However, as
36 the peak of the mean seasonal cycle of TCs lags two months behind that of the
37 EASM, the moisture transported by TCs is an important source for the water
38 budget over the EA region when the EASM withdraws. This moisture trans-
39 port is largely performed by westward-moving TCs. These results improve
40 our understanding of the water cycle of EA and provide a useful test bed for
41 evaluating and improving seasonal forecasts and coupled climate models.

1. Introduction

East Asia (EA) is affected by one of the most intense monsoon systems; its rainfall and water budget are dominated by the East Asia summer monsoon (EASM). Meanwhile, the Western North Pacific (WNP) basin and the coast of EA are regions that have the most frequent impacts from tropical cyclones (TCs). Landfall of TCs is accompanied by destructive winds, storm surges and heavy rainfall that threatens the lives and socioeconomic systems of hundreds of millions of people living along the EA coast. Forming over the western Pacific warm pool, TCs that move across the EA region bring warm and moist air into land. TCs, therefore, could be a key contributor to the rainfall and water budget over the EA, especially over China. Quantifying these contributions of TCs would improve understanding and prediction of water cycle variability over the EA, which is essential to agriculture and the local economy.

TC variability has been extensively studied on a variety of temporal scales. Over the WNP and EA regions, studies have covered scales from intra-seasonal to decadal. TC variability has been linked with the Madden–Julian Oscillation (Feng et al. 2013; Kim et al. 2008; Camargo et al. 2007b), the El Niño–Southern Oscillation (Chan 2000; Wang and Chan 2002; Chia and Ropelewski 2002; Camargo et al. 2007a), the Quasi-Biennial Oscillation (Ho et al. 2009) and the Pacific Decadal Oscillation (Lee et al. 2012). In general, there are several key aspects of the background state and large-scale circulation over the EA that have been linked to TCs on different temporal scales, e.g., sea surface temperature (SST), vertical wind shear, and the positions and intensities of the monsoon trough/Intertropical Convergence Zone (ITCZ) and the Western North Pacific Subtropical High (WNPSH).

While the drivers of TC variations over EA have been widely studied, the contributions of TCs to the EA water cycle have received less attention, even in terms of their climatologies. Contributions

of TCs to total and extreme rainfall over the EA have been investigated using gauge data (Chen et al. 2010, 2012; Ren Fumin 2002; Ren et al. 2006; Wu et al. 2007; Wang and Chen 2008). A typical contribution of TCs to the total annual rainfall along the southeastern coastal region is 20–40%, with the largest impact over Hainan Island off the south China coast (Ren et al. 2006; Wu et al. 2007). During the second half of the 20th century, the number of TCs that affect China shows a downward trend, which is accompanied by a decreasing trend in the contribution of TC rainfall to the total rainfall (Ren et al. 2006). Over Taiwan Island, TC rainfall accounts for 40% of total rainfall during late summer to early autumn (Wang and Chen 2008). Over other TC-active regions, the contribution of TC rainfall to the total rainfall varies; however, along the coastal regions, the TC rainfall contribution is 10–40% (Prat and Nelson 2013; Dare et al. 2012; Prat and Nelson 2016). The contribution of TCs to Australian extreme rainfall and to United States flooding has been analysed by Villarini and Denniston (2015) and Villarini et al. (2014). Over Australia, more than half of the highest annual rainfall events associated with TCs are over the coastal regions and in particular in Western Australia (Villarini and Denniston 2015). TC rainfall accounts for 20–40% of total rainfall over northwest Australia during the Southern Hemisphere warm season (Dare et al. 2012). TC rainfall is also a major cause of floods in the eastern United States (Villarini et al. 2014). There are about 14% of total onshore flux over the coast of the North America is attributed to the Atlantic TCs (Xu et al. 2016).

The aforementioned studies suggest that TCs have the potential to make a substantial contribution to the water cycle over EA. The fact that TC contributions to the atmospheric moisture budget have received little attention may be explained by the perceived dominance of the EASM, one of the most intense monsoon systems on the planet. The water budget is thus dominated by the EASM, which explains why most studies have been concentrating on this aspect, while the role played by TCs in the water cycle has been neglected. This study is therefore an attempt to the gap

between studies of the impact of TCs on rainfall and those of the role of the EASM in the moisture budget. As our study will show, due to differences in the timing of the seasonal cycles of TCs and the EASM, the contribution of TCs to the water cycle is non-negligible, even compared to the substantial transport by the EASM, and is particularly important to the EA during the EASM withdrawal phase.

In this study, we decompose the total rainfall and moisture transport into contributions from TCs and from the mean flow. Then, we calculate the contributions of TCs to the rainfall and water budgets and compare these with the EASM in terms of climatology. Data and methods are introduced in Section 2; the statistics of TCs over the EA are shown in Section 3; TC contributions to both total and extreme rainfall are discussed in Section 4; the comparison of moisture transport from TCs with that from the EASM is shown in Section 5. Finally, the conclusion and discussion are given in Section 6.

2. Data and Methods

a. Observation and Re-analysis data

To evaluate the contribution of TCs to rainfall over the EA, we use the satellite-derived Tropical Rainfall Measuring Mission (TRMM) 3B42 version 7 (v7) rainfall analyses (Huffman and Bolvin 2012). It is a 3-hourly $0.25^\circ \times 0.25^\circ$ gridded rainfall dataset produced from 1998 onwards. The spatial coverage is $50^\circ\text{S} - 50^\circ\text{N}$, $180^\circ\text{W} - 180^\circ\text{E}$. Chen et al. (2013) showed that TRMM 3B42 v7 has improved skill at detecting intense TC rainfall, with good correlations and spatial patterns that agree with rain gauge observations. This skill is higher over ocean than land, and it is least skilful over land with high elevation. Therefore, we will interpret our results with caution.

110 The ERA-Interim re-analysis dataset (Berrisford et al. 2011; Dee et al. 2011) from the European
111 Centre for Medium-Range Weather Forecasts (ECMWF) is used in this study for TC trajectory
112 identification and moisture transport calculations. It produces 6-hourly analyses at 00, 06, 12, 18
113 UTC. Variables used in this study include temperature, winds, vorticity and specific humidity on
114 pressure levels and vertically integrated moisture fluxes and their divergence. Variables provided in
115 the original truncation (truncation at wavenumber 255; T255) are used to identify TC trajectories;
116 variables for the moisture transport calculations are gridded onto a 512 longitude \times 256 latitude
117 regular grid with a resolution of $0.7^\circ \times 0.7^\circ$.

118 *b. TC feature tracking methodology*

119 TC trajectories used in this study are obtained from an objective feature tracking method. This
120 method has been developed and described fully in Hodges (1994, 1995, 1999) and Bengtsson
121 et al. (2007). The method is applied to 6-hourly ERA-Interim re-analysis data. It uses the vertically
122 averaged vorticity at the levels 850, 700 and 600 hPa and truncated to T63 with the planetary scales
123 removed (total wave-number $n \leq 5$). This was found to provide more coherent tracks including
124 the pre-TC stages (e.g., Easterly Waves) and post-TC stages following extra-tropical transition
125 (Serra et al. 2010; Hodges and Emerton 2015). At this stage all tropical disturbances are tracked.
126 To identify TCs, additional information is added to the tracks in the form of vorticity at T63
127 resolution at multiple levels across 850–250 hPa. This allows for checking for the presence of a
128 warm core and a coherent vertical structure. The criteria used for checking are the same as used
129 in Bengtsson et al. (2007) and other studies (Strachan et al. 2013; Bell et al. 2013; Roberts et al.
130 2015).

131 TC tracks identified from the ERA-Interim reanalysis have been compared with observations
132 in previous studies. The average annual TC numbers identified from the ERA-Interim reanalysis

agree well with the International Best Track Archive for Climate Stewardship (IBTrACS) over the period of 1979-2002 (Strachan et al. 2013). A recent study by Hodges and Vidale (personal communication) matches TC tracks identified from the ERA-Interim reanalysis to the IBTrACS data in 1979-2012. 95% of the TCs in the IBTrACS data are identified in the ERA-Interim reanalysis in the Northern Hemisphere and 93% in the Southern Hemisphere. The interannual variability of TC numbers is also well correlated between the ERA-Interim reanalysis and the IBTrACS data. Over the Western Pacific region, the correlation coefficient is 0.57, which is significant at the 95% confidence level; the correlation coefficients are similar or higher over other TC basins, e.g., the North Atlantic and the South Indian Ocean (Strachan et al. 2013). The lower correlation coefficient over the Western Pacific region compared to other regions is largely due to uncertainties of identifying the weaker storms. This is partly due to the tracking method and the uncertainties in the ERA-Interim reanalysis, but there may also be contributions from uncertainties in the observations for weak storms and whether reporting agencies are consistent in the types of storms they include in the TC datasets used for IBTrACS (Hodges and Vidale 2017). The spatial distribution of TC tracks identified from the ERA-Interim reanalysis also agrees well with the IBTrACS. Strachan et al. (2013) shows strong agreement between the ERA-Interim reanalysis and the IBTrACS in terms of TC track density, as well as TC genesis and lysis density.

c. Decomposition of mean-flow and eddy moisture fluxes related to TCs

To investigate the contribution of TCs to moisture transport over the EA, first the moisture flux is decomposed into time-mean and eddy (deviation from the mean) terms, using the 6-hourly ERA-Interim re-analysis during 1979–2012 (Eq. 1). In Eq. 1, \mathbf{v} is horizontal wind, q is the specific humidity, both are available on the 6-hourly time interval during 1979–2012; $\bar{\mathbf{v}}$ and \bar{q} are monthly climatologies over 1979–2012, \mathbf{v}' and q' are eddies (or deviations from the time-mean values)

156 calculated as $\mathbf{v}' = \mathbf{v} - \bar{\mathbf{v}}$ and $q' = q - \bar{q}$ using 6-hourly ERA-Interim re-analysis. The first term on
 157 the righthand side of Eq. 1, $\bar{\mathbf{v}} \cdot \bar{\mathbf{q}}$, is the transport of mean moisture by the mean horizontal wind.
 158 We call this term the mean moisture transport or the mean-flow moisture flux afterwards. The
 159 second to the fourth terms, $\bar{\mathbf{v}} \cdot \mathbf{q}'$, $\mathbf{v}' \cdot \bar{\mathbf{q}}$ and $\mathbf{v}' \cdot \mathbf{q}'$, are the transport of eddy moisture by the mean
 160 horizontal wind, the transport of mean moisture by the eddy horizontal wind and the transport of
 161 eddy moisture by the eddy horizontal wind, respectively. Altogether, we call these terms the eddy
 162 moisture transport or eddy moisture flux. Then, by using the TC location information obtained
 163 from the feature tracking method, a mask with a 5° geodesic radius around each TC eye at each
 164 6-hr time step is applied to the eddy terms to identify eddies that are related to the TC and mask
 165 out those that are not related (Eq. 2). Therefore, the eddy terms in Eq. 1 are further decomposed
 166 into TC-related terms and non-TC related terms in Eq. 2. In the following analysis, we focus on
 167 the mean-flow moisture flux and the eddy moisture fluxes that are related to TCs. Although the
 168 size of a TC varies from storm to another, the choice of a 5° radius is an established method of
 169 differentiating TC-related features from their surroundings that has been discussed and applied by
 170 previous studies (Englehart and Douglas 2001; Larson et al. 2005; Jiang and Zipser 2010; Prat and
 171 Nelson 2013).

$$\begin{aligned}
 \mathbf{v} \cdot \mathbf{q} &= (\bar{\mathbf{v}} + \mathbf{v}') \cdot (\bar{\mathbf{q}} + \mathbf{q}') \\
 &= \bar{\mathbf{v}} \cdot \bar{\mathbf{q}} + \bar{\mathbf{v}} \cdot \mathbf{q}' + \mathbf{v}' \cdot \bar{\mathbf{q}} + \mathbf{v}' \cdot \mathbf{q}'
 \end{aligned} \tag{1}$$

$$\begin{aligned}
 \mathbf{v} \cdot \mathbf{q} &= (\bar{\mathbf{v}} + \mathbf{v}'_{\text{TC}} + \mathbf{v}'_{\text{non-TC}}) \cdot (\bar{\mathbf{q}} + \mathbf{q}'_{\text{TC}} + \mathbf{q}'_{\text{non-TC}}) \\
 &= \bar{\mathbf{v}} \cdot \bar{\mathbf{q}} + \underbrace{\bar{\mathbf{v}} \cdot \mathbf{q}'_{\text{TC}} + \mathbf{v}'_{\text{TC}} \cdot \bar{\mathbf{q}} + \mathbf{v}'_{\text{TC}} \cdot \mathbf{q}'_{\text{TC}}}_{\text{TC related}} \\
 &\quad + \underbrace{\bar{\mathbf{v}} \cdot \mathbf{q}'_{\text{non-TC}} + \mathbf{v}'_{\text{non-TC}} \cdot \bar{\mathbf{q}} + \mathbf{v}'_{\text{non-TC}} \cdot \mathbf{q}'_{\text{non-TC}}}_{\text{non TC related}}
 \end{aligned} \tag{2}$$

172 Similar to the method for decomposing the moisture flux, the mask with 5° geodesic radius
173 around each TC eye at each time step is also applied to 3-hourly TRMM 3B42 rainfall to separate
174 TC-related rainfall from non-TC-related rainfall. Note that the temporal interval of the tracked
175 TC position is 6 hours; therefore when filtering 3-hourly TRMM 3B42 rainfall, the same mask is
176 applied to two consecutive time steps of TRMM rainfall. We assume that the movement of a TC
177 is small within 6 hours, relative to the diameter of the masking circle.

178 The extreme daily rainfall on each grid is defined as the daily rainfall above the 95th percentile
179 of rainfall in each month during 1998–2012.

180 **3. Statistics of TCs over East Asia**

181 There are 851 TCs tracked over the WNP and EA during 1979–2012. These TCs are divided into
182 two groups according to their propagation directions: westward and northward. The westward-
183 moving TCs are generated over the Pacific warm pool east of the Philippines, then move west-
184 ward/northwestward in a straight line and make landfall along the coasts of south China or the
185 Indochina peninsula. The northward-moving TCs are also generated over the Pacific warm pool,
186 but instead of hitting the coast and moving further west, these TCs curve toward the north and
187 make landfall over the eastern China, the Korean peninsula or Japan. This division is similar to
188 that in Camargo et al. (2007a), who used cluster analysis to divide TC trajectories over the WNP
189 and EA into seven clusters which can be further grouped as straight-movers and recurvers. In
190 general, westward-moving TCs are similar to the straight-movers in Camargo et al. (2007a), and
191 northward-moving TCs are similar to the recurvers. Camargo et al. (2007a) found that the seven
192 clusters in their analysis show different characteristics in terms of genesis position and lifetime.
193 However, when comparing the difference in landfall locations, the seven clusters merged into two
194 groups according to their trajectories (straight-mover or recurver). As we focus on the contribu-

tion of TCs to precipitation and moisture fluxes over the EA landmass, this remerging of the seven clusters into two groups based on landfall location, gives us confidence to use the much simpler straight-mover/recurver (westward/northward) classification to carry out our study.

The number of TCs in each month and in each group over the period of 1979–2012 is shown in Figure 1. There are more northward-moving TCs than westward-moving TCs in each month, which is consistent with results shown in other datasets e.g., IBTrACS (Camargo et al. 2007a). TC activity over the WNP and EA shows a single peak in the mean seasonal cycle. More in detail, westward-moving TCs are rare from January to May, then increase from July to October (JASO) with the highest number in October; northward-moving TCs show a similar seasonal cycle, being inactive from December to April and active during JASO, with the highest number occurring in September. 58% of all TCs over the WNP and EA occur during JASO. After peaking, TC activity over the WNP and EA decreases rapidly.

These seasonal features over the WNP and EA are similar to those for global TCs, which are due to a number of factors, e.g., the mean seasonal cycle SST, which is positively correlated with mean seasonal cycle of TC frequency; a low vertical wind shear in the atmosphere and the existence of a monsoon trough or easterly waves. However, other features, such as the division of westward and northward trajectories, are unique and relate to the positions of the EA summer monsoon trough and the WNPSH. We find similar statistics to 1979–2012 for the 1998–2012 period of the TRMM rainfall record (not shown). During season JASO, there are 14.6 TCs/season over the period 1979–2012 and 14.0 TCs/season over the period 1998–2012.

4. Fractional contribution to rainfall

The monthly mean fractional contribution of TC rainfall to total rainfall during 1998–2012 is shown in Figure 2. TC rainfall makes larger fractional contributions during JASO over both the

218 WNP and the coast of the EA. In other months, the TC contribution is small and confined to the
219 WNP warm pool. Only the Indochina peninsula is affected by TCs in November–January. Note
220 that there are some spotted contributions over the mid-latitudes in December–February. This is
221 caused by mid-latitude disturbances that have been identified as TCs and thus been included in the
222 analysis here. However, the contributions from these mid-latitude disturbances are negligible.

223 During JASO, the average contribution of TC rainfall over the southeastern coast of China is 10–
224 30%. The contribution is larger at lower latitudes, especially over islands, e.g., Taiwan, Hainan
225 island and the Philippines, where the contribution is as high as 40–50%. At higher latitudes, e.g.,
226 the Bohai Bay, the Korean Peninsula and the southern Japan, TCs make a substantial contribution
227 to total rainfall only in August and September. The spatial pattern of the contribution of TC
228 rainfall matches closely with the TC number shown in Figure 1. With most northward-moving TCs
229 occurring in September, the impact of TCs reaches as far north as 45°N in that month; since most
230 westward-moving TCs occur in October, the TC rainfall contribution also reaches its maximum
231 over the Indochina peninsula in October.

232 Heavy rainfall caused by TCs after landfall can cause flooding and other losses. Therefore,
233 it is necessary to quantify the TC contribution to extreme rainfall over the EA. We define an
234 extreme rainfall day as the occurrence of daily rainfall above a threshold of the 95th percentile;
235 the threshold is computed for each month and gridpoint using data for 1998–2012. We compute
236 the contribution of TCs to both the occurrence and amount of extreme rainfall during JASO. (In
237 other months, these contributions are negligible over the EA.) For occurrence, at each gridpoint
238 we compute the percentage of extreme rainfall days on which a TC is within the area defined by a
239 circle with a 5° geodesic radius around that gridpoint. If there were no relationship between TCs
240 and extreme rainfall occurrence, this percentage would be 5%. For amount, at each gridpoint we
241 compute the percentage of the total amount of extreme rainfall (summed over all extreme days) that

occurs on TC days. The contribution of TCs to extreme rainfall occurrence is shown in the upper panels of Figure 3. In general, the contribution of TCs to extreme rainfall occurrence is higher than to total rainfall, which indicates that rainfall intensity during TCs is above average. Over the ocean, the contribution to occurrence is over 70%, which means that on over 70% of days on which daily rainfall exceeds the 95th percentile there is a TC within a 5°-radius of the grid-point; this contribution is over 90% in September and October, especially to the east of Taiwan and the Philippines. Over Taiwan, TCs appear on more than 70% of extreme rainfall days; this contribution can also reach 60% over Hainan island and the northern Philippines. Along the southern China coast and the Indochina peninsula, this contribution is also over 50%, which is higher than the TCs contribution to total rainfall.

The contribution of TCs to extreme rainfall amount is shown in the lower panel of Figure 3. Comparing the TC contributions to occurrence and amount allows us to measure whether extreme rainfall related to TCs is heavier than extreme rainfall that is unrelated to TCs. If this were the case, then the TC contribution to extreme rainfall amount would be higher than the contribution to extreme rainfall occurrence. As shown in Figure 3, the spatial distribution of contributions to extreme rainfall amount is similar to the contributions to extreme rainfall occurrence (the pattern correlation between maps of these diagnostics for each month varies between 0.8 and 0.99). However, there are regions where the contributions to extreme rainfall amount are higher than the contributions to extreme rainfall occurrence. For example, over the Anhui Province of China (30°N, 117°E) in September, the contributions to extreme rainfall occurrence are about 30–40%, while the contributions to extreme rainfall amount are about 50%. This difference indicates that TC-related extreme rainfall over these regions is heavier than extreme rainfall that is unrelated to TCs.

5. Moisture flux: relative contributions of eddy (TC) transport and mean flow

As EA is affected by one of the most prominent monsoon systems, the warm and moist monsoonal flow brings a large amount of moisture over land. Generated over the warm and moist ocean, TCs also gather and transport moisture along their paths. With TC landfalls, moisture convergence associated with TCs is therefore a contributor to the water budget over the EA.

To compare the roles of TCs and the EASM in the process of moisture transport, Figure 4 shows monthly accumulated moisture flux divergence due to both the mean, $\nabla \cdot (\bar{\mathbf{v}} \cdot \bar{\mathbf{q}})$, and the TC eddy moisture transport, $\nabla \cdot (\bar{\mathbf{v}} \cdot \mathbf{q}'_{\text{TC}} + \mathbf{v}'_{\text{TC}} \cdot \bar{\mathbf{q}} + \mathbf{v}'_{\text{TC}} \cdot \mathbf{q}'_{\text{TC}})$. The mean-flow moisture flux divergence shows features arising from the EASM (the upper panel of Figure 4), i.e., a moisture convergence band which represents the Mei-Yu front (shown in Figure 4 by the ridge of the WNPSH at 500 hPa) stretches from central China to Japan in July and August, then shifts southward to the southern China in September; the band then withdraws further south to the Indochina Peninsula in October and eventually fades away from the most of the EA landmass.

The TC eddy moisture flux divergence is smaller in amplitude and also in spatial extent compared to the mean-flow moisture flux divergence (the lower panel of Figure 4). However, TC moisture flux divergence shows a different seasonal cycle from the mean EASM moisture flux divergence, i.e., the mean-flow moisture flux convergence prevails over the EA during JJA, while the TC moisture flux convergence affects the EA during JASO. The spatial patterns of moisture flux convergence are also different between the EASM and TCs. The position of the Mei-Yu front, where the mean-flow moisture flux convergence dominates, depends on the positions of the monsoon trough and the ridge of the WNPSH, while the pattern of TC moisture flux convergence depends on the number and trajectories of TCs.

Therefore, the TC moisture flux convergence is not negligible with respect to the mean-flow moisture flux convergence; their contributions to the water cycle come in different regions and at different times. In July, when the Mei-Yu front is located at around 30°N , the mean-flow moisture flux comes from the south and converges along the Mei-Yu front. Meanwhile, southern China loses moisture due to mean-flow moisture flux divergence. However, for TCs, there are more westward-moving TCs moving into southern China in July, which import moisture that is required to maintain rainfall over this region. In August, when the intensity of the NWPSH weakens and the Mei-Yu front deflects to the south, the mean-flow moisture flux convergence becomes the main moisture supplier over southern China again. For TCs, there are more northward-moving TCs in August, which bring moisture to higher latitudes including the Baohai Bay, Korean Peninsula and Japan; the TC moisture flux replaces the mean-flow moisture flux as the main supplier of moisture over the northern China. TCs reach their peak in September, when the mean-flow moisture flux weakens and the Mei-Yu front withdraws further south to the south coast of China and the Indochina Peninsula, and play a more important role in transporting moisture to the north. In October, when the EASM has completely faded away from the EA, TCs remain as the main moisture supplier to the EA, especially along the coast. TCs are able to transport moisture beyond the coastal regions to further inland, but their reach does not extend as far inland as that of the mean flow.

The seasonal cycle of monthly mean vertically integrated moisture flux passing through the coastal boundaries of the EA is shown in Figure 5. Two boundaries are defined, shown in the inner panel of Figure 5: an eastern (meridional) boundary at 121°E between 21° - 43°N , and a southern (zonal) boundary at 21°N between 100° - 121°E . Because there is little moisture transported from the north, we do not use a northern boundary. Although there is significant mean moisture transported from the west during the Indian monsoon season, the TC moisture transported from the

311 west remains small as most TCs move westward or northward over the EA. Therefore, moisture
312 transported into the EA region from the west is not included in this comparison of the mean flow
313 and TCs.

314 The seasonal cycles of the mean-flow moisture fluxes on both boundaries show a clear EASM
315 cycle. At the southern boundary, moisture is transported into the EA between February and Au-
316 gust. This period can be further divided into two sub-phases. From late February to early May,
317 the mean-flow moisture influx is small and supplies moisture for the Spring Rainfall (Tian and
318 Yasunari 1998) over southeastern China; from late May to August, the mean-flow moisture influx
319 increases and supplies moisture for the EASM. This moisture is brought in by both the westerly
320 flow from the Indian Ocean, extending from the Indian monsoon circulation, and the western flank
321 of the WNPSH, which are the dominant features defining the EASM. From September to Decem-
322 ber, the winter monsoon brings dry and cold air from the north, and the mean-flow moisture flux at
323 the southern boundary is negative. At the eastern boundary, the mean-flow moisture flux is almost
324 opposite to that at the southern boundary. Moisture imported to the EA via the southern boundary
325 is exported from the eastern boundary. This outflow is particularly important to several East Asian
326 regions, i.e. the Korean Peninsula and Japan, as it is the main moisture supply during JJA.

327 The TC moisture fluxes on both boundaries are an order of magnitude smaller than the mean
328 fluxes. However, the seasonal cycles of TC moisture fluxes on both boundaries are different
329 from the mean-flow fluxes. In general, instead of showing a maximum moisture flux during JJA,
330 TC moisture fluxes peak during JASO, consistent with the seasonal distribution of TC frequency
331 shown in Fig 1. Instead of gaining moisture from the southern boundary and losing moisture from
332 the eastern boundary like the mean-flow moisture fluxes, the direction of TC moisture fluxes is
333 opposite. That is, TC moisture flux causes a net import at the eastern boundary and a net export at
334 the southern boundary.

335 To understand this difference in moisture transport between the mean flow and TCs, case studies
336 for different types of TCs are carried out. Figure 6 shows the total TC moisture fluxes and their
337 divergence for two different TCs: a westward-moving TC (Tai-Kat) and a northward-moving TC
338 (Masta). In a single time step, the TC moisture flux shows a cyclonic circulation with predominant
339 convergence (not shown). As the TC moisture flux is summed along its trajectory (multiple time
340 steps) for either a westward-moving or a northward-moving TC, the cumulative TC moisture flux
341 is modified due to the partial overlap of the 5° circles around the TC on consecutive timesteps, i.e.,
342 the front of a TC in its direction of travel at the n th time step is overlapped by the rear part of a TC at
343 the $n + 1$ th time step. Due to the cyclonic flow around the TC, the direction of the wind (and hence
344 the moisture transport) reverses, such that the cumulative TC moisture flux is weakened in the TC
345 area along the trajectory. Meanwhile, TC moisture fluxes at the edges of the TC area orthogonal
346 to the direction of propagation remain strong or even are strengthened, because the moisture flux
347 retains its sign as the TC propagates. As shown in Figure 6, there are strong forward fluxes (same
348 direction as the TC propagation direction) to the right of a TC, and strong rearward flux (opposite
349 direction to the TC propagation direction) to the left of a TC. This is the case for either westward-
350 moving TCs or northward-moving TCs. As most westward-moving TCs appear to the south of
351 the EA landmass (between 15° - 25° N, as shown in Figure 8), the south/southeast coast of China is
352 exposed to the easterly moisture flux prevailing to the right of these TCs. Therefore, TC moisture
353 fluxes enter the EA region from the eastern boundary during the active period (JASO).

354 A similar argument applies to the northward-moving TCs and moisture export from the southern
355 boundary. With northward-moving TCs approaching the coast of EA, the northerly moisture flux
356 to the left of the direction of propagation of these TCs has a large impact. Therefore, there is an
357 export of moisture at the southern boundary during the TC active period. Note that the moisture
358 export at the southern boundary is smaller than the moisture import at the eastern boundary. This

could be because the propagation direction of TCs and the direction of moisture flux are opposite to each other at the southern boundary, which reduces the intensity of moisture flux. This could also be because the moisture flux at the southern boundary is weaker than the moisture flux at the eastern boundary due to drier air. The easterly moisture flux at the eastern boundary is imported directly from the warm and humid ocean, but the northerly moisture flux at the southern boundary is exported from the EA landmass. After weakening and drying as a result of the rough land surface and the lack of moisture supply from the ocean, the TC intensity is reduced. For all these reasons, only a fraction of moisture is exported at the southern boundary compared to the moisture imported at the eastern boundary.

We also note that the export of moisture at the southern boundary disappears after August and changes sign in September. This is due to changes in the background meridional specific humidity gradient (Figure 7). The mean specific humidity field shows a reversed meridional gradient during JJA (i.e., higher humidities in the subtropics than at the equator), and a normal meridional gradient before and after JJA. The reversed specific humidity gradient is due to the strong mean moisture flux convergence and high land surface temperature over the EA during the EASM. As shown in Equation 2, the TC eddy moisture flux is composed of three terms ($\bar{\mathbf{v}} \cdot \mathbf{q}' + \mathbf{v}' \cdot \bar{\mathbf{q}} + \mathbf{v}' \cdot \mathbf{q}'$). Among them, the second term (i.e., the mean specific humidity transported by TC eddies) dominates (not shown). Therefore, when comparing the TC moisture flux in August and September, though the TC eddies themselves are similar in structure, the TC moisture flux changes its sign due to the reversed moisture meridional gradient.

Another interesting point is that, as shown in Figure 8, although September and October feature more westward-moving TCs (57 and 62 TCs, respectively), the TC moisture flux transport through the eastern boundary is smaller compared to that of August or July, which have 40 or 52 westward-moving TCs, respectively. This is due to the seasonal shift of TC locations: any TC that contributes

383 to moisture flux on the eastern boundary needs to be located north of 16°N between 100° - 121°E
384 (the dotted line in Figure 8). In September, 54% of the westward-moving TCs appear to the north
385 of this line, and this proportion decreases to 24% in October. Although there are fewer total
386 westward-moving TCs in July and August, there are more westward-moving TCs north of 16°N
387 (90% in July and 73% in August). The range and position of WNPSH shown in Figure 4 also
388 indicate changes in background circulation that contribute to this shift. In October, the WNPSH
389 locates at lower latitude and is elongated from the east of Philippine westward to reach the Indo-
390 China Peninsula. The easterlies along the southern flank of the WNPSH favour more westward-
391 moving TCs, and because of its low latitude, more TCs are located to the south of 16°N .

392 **6. Conclusion and Discussion**

393 This study was motivated by the need to quantify the contributions of TCs to the water budget
394 over the EA, especially over China. Previous studies in this field focus either on the drivers of
395 TC variability on temporal scales from intra-seasonal to decadal, or on the contribution of TCs to
396 rainfall. This study is therefore an attempt to bridge the gap between studies that investigate TC
397 variations and studies that focus only on the TC contribution to rainfall over the EA. This study
398 retains its focus on the climatological contributions of TCs atmospheric moisture transport, as well
399 as extreme and total rainfall. We found a distinct seasonal cycle and direction of moisture transport
400 by TCs when compared to the mean moisture transport associated with the EASM.

401 In this study, TC tracks over the WNP and EA were first identified by applying an objective
402 feature tracking method to the ERA-Interim 6-hourly re-analysis (1979–2012). Compared with
403 the observation dataset IBTrACS, the correspondence between these two data is 95-98% over the
404 Western North Pacific and East Asia (Strachan et al. 2013; Roberts et al. 2015). According to
405 TC tracks, TCs over the WNP and EA are separated into two groups according to propagation

direction: the westward and northward-moving TCs. The TC seasonal frequency histograms from 1979–2012 show that JASO is the active season for both groups of TCs, accounting for 58% of the overall number over the WNP and EA.

Consistent with the seasonal cycle in TC numbers, during JASO, TC rainfall has the largest contribution over the EA coast, with an averaged contribution between 10–30% of the total rainfall. TC rainfall reaches as far north as 45°N in September for the northward-moving TCs and has its maximum impact over the Indochina peninsula for the westward-moving TCs in October. TC rainfall contribution is largest over the tropical islands, i.e., Taiwan, the Philippines and Hainan island, with contributions as high as 50% of the total rainfall.

TC rainfall contributions to the extreme daily rainfall (above the 95th percentile) are investigated in terms of occurrence and amount. The contribution of TCs to the occurrence of extreme daily rainfall is around 50% over the EA coast. This contribution is higher (60–70%) over tropical islands. The TC contribution to the extreme rainfall amount is higher in percentage than the contribution to the extreme rainfall occurrence over some regions, e.g., the Anhui Province of China along the Yangtze River Valley. This indicates that TC-related extreme rainfall over these regions is heavier than extreme rainfall unrelated to TCs.

Due to different seasonal cycles, moisture transport associated with TCs is another important source for the water budget of the EA, although its magnitude is smaller than the mean-flow moisture transport associated with the climatological EASM. The mean-flow moisture transport reaches a maximum during JJA and features a moisture convergence band (the Mei-Yu front) marching north in July and gradually withdrawing to the south in the following months. The TC moisture transport reaches a maximum during JASO; it is an important moisture supplier especially after the EASM withdraws.

429 The pathways of moisture flux transported by the mean flow and TCs also show different pat-
430 terns. For the mean flow, moisture is imported from the south and exported to the east with its
431 maximum during the EASM season (JJA). For TCs, moisture is imported from the east and ex-
432 ported to the south during the TC active season (JASO). This different pattern of TC moisture
433 transport is closely related to TC propagation directions, changes in the mean meridional humidity
434 gradient and the shift of TC positions with large-scale background flow during the season.

435 The diagnostics conducted in the study have been repeated with the IBTrACS data and show
436 similar results. Quantitative differences, however, are found. The TC moisture fluxes via both
437 boundaries (as defined in Figure 5) are larger by using the IBTrACS data. It is about 20% larger
438 for the TC moisture influx via the eastern boundary during the TC peak season. The difference
439 in the net TC moisture flux is less than 10% due to the larger TC moisture efflux via the southern
440 boundary during the TC peak season. And, the sign change of TC moisture flux in September
441 on the southern boundary is delayed to October while using the IBTrACS tracks. Nevertheless,
442 results from both TC tracks support the same conclusions.

443 A major aim of this study was to identify and quantify the contribution of TCs to rainfall and
444 the water budget over the EA, especially China. However, simulating rainfall over the EA remains
445 a challenge for state-of-the-art general circulation models (GCMs) (Sperber et al. 2013; Song and
446 Zhuo 2014). As TCs make an important contribution to the rainfall and water budget over the EA,
447 it is essential that models represent accurately not only the characteristics of TCs themselves, but
448 also their impacts on the large-scale atmospheric environment. The TC feature tracking method
449 used in this study offers an opportunity to compare TC activity in model simulations to reanalysis
450 data using an identical method. It will be valuable to assess model simulations using the analysis
451 techniques developed this study, especially for sensitivity tests with a single model (e.g., tests of
452 horizontal resolution or of atmosphere-ocean feedbacks). Roberts et al. (2015) (and references

therein) showed that model resolution is crucial for a realistic simulation of TC behaviour and variability, and higher resolution GCMs are increasingly able to capture TC intensity and the large-scale environmental conditions that contribute to tropical cyclogenesis. To further understand the water budget over this region, contributions from other components need to be quantified. This will also help to identify deficits in model simulations and improve the skill of climate prediction and weather forecasting over this region.

Acknowledgments. The authors thank Kevin Hodges for discussions and comments, especially on the feature checking methodology; the authors appreciate discussions with Malcolm Roberts. This work and its contributors were supported by the UK-China Research & Innovation Partnership Fund through the Met Office Climate Science for Service Partnership (CSSP) China as part of the Newton Fund. NPK was also funded by a UK Natural Environment Research Council Independent Research Fellowship (NE/L010976/1).

References

- Bell, R., J. S. P. L. Vidale, K. Hodges, and M. Roberts, 2013: Response of Tropical Cyclones to Idealized Climate Change Experiments in a Global High-Resolution Coupled General Circulation Model. *Journal of Climate*, **26** (20), 7966–7980, doi:10.1175/JCLI-D-12-00749.1.
- Bengtsson, L., K. I. Hodges, and M. Esch, 2007: Tropical cyclones in a T159 resolution global climate model: Comparison with observations and re-analysis. *Tellus*, **59A**, 396–416, doi:10.1111/j.1600-0870.2007.00236.x.
- Berrisford, P., and Coauthors, 2011: REA-Interim archive, v2. Tech. Rep. 23, ECMWF, UK. URL <http://old.ecmwf.int/publications/library/do/references/show?id=90276>.

- 474 Camargo, S. J., A. W. Robertson, S. J. Gaffney, P. Smyth, and M. Ghil, 2007a: Cluster Analysis
475 of Typhoon Tracks. Part I: General Properties. *Journal of Climate*, **20**, 3635–3653, doi:dx.doi.
476 org/10.1175/JCLI4188.1.
- 477 Camargo, S. J., A. W. Robertson, S. J. Gaffney, P. Smyth, and M. Ghil, 2007b: Cluster Analysis
478 of Typhoon Tracks. Part II: Large-Scale Circulation and ENSO. *Journal of Climate*, **20**, 3654–
479 3676, doi:dx.doi.org/10.1175/JCLI4203.1.
- 480 Chan, J. C. L., 2000: Tropical Cyclone Activity over the Western North Pacific Associated
481 with El Nio and La Nia Events. *Journal of Climate*, **13**, 2960–2972, doi:dx.doi.org/10.1175/
482 1520-0442(2000)013<2960:TCAOTW>2.0.CO;2.
- 483 Chen, J., R. Wu, and Z. Wen, 2012: Contribution of South China Sea Tropical Cyclones to an
484 Increase in Southern China Summer Rainfall Around 1993. *Advances in Atmospheric Science*,
485 **29 (3)**, 585–598, doi:10.1007/s00376-011-1181-6.
- 486 Chen, J.-M., T. Li, and C.-F. Shih, 2010: Tropical Cyclone and Monsoon-Induced Rainfall Vari-
487 ability in Taiwan. *Journal of Climate*, **23**, 4107–4120, doi:10.1175/2010JCLI3355.1.
- 488 Chen, Y., E. E. Ebert, K. J. Walsh, and N. E. Davidson, 2013: Evaluation of TRMM 3B42 pre-
489 cipitation estimates of tropical cyclone rainfall using PACRAIN data. *Journal of Geophysical*
490 *Research*, **118 (5)**, 2184–2196, doi:10.1002/jgrd.50250.
- 491 Chia, H., and C. Ropelewski, 2002: The interannual variability in the genesis location of
492 tropical cyclones in the northwest Pacific. *Journal of Climate*, **15 (20)**, 2934–2944, doi:
493 10.1175/1520-0442(2002)015<2934:TIVITG>2.0.CO;2.

494 Dare, R. A., N. E. Davidson, and J. L. McBride, 2012: Tropical Cyclone Contribution
 495 to Rainfall over Australia. *Monthly Weather Review*, **140** (11), 3606–3619, doi:10.1175/
 496 MWR-D-11-00340.1.

497 Dee, D. P., and Coauthors, 2011: The ERA-Interim reanalysis: configuration and performance of
 498 the data assimilation system. *Quarterly Journal of the Royal Meteorological Society*, **137** (656),
 499 553–597, doi:10.1002/qj.828.

500 Englehart, P. J., and A. V. Douglas, 2001: The role of eastern North Pacific tropical storms in the
 501 rainfall climatology of western Mexico. *International Journal of Climatology*, **21** (11), 1357–
 502 1370, doi:10.1002/joc.637.

503 Feng, X., R. Wu, J. Chen, and Z. Wen, 2013: Factors for Interannual Variations of Septem-
 504 berOctober Rainfall in Hainan, China. *Journal of Climate*, **26** (22), 8962–8978, doi:10.1175/
 505 JCLI-D-12-00728.1.

506 Ho, C.-H., H.-S. Kim, J.-H. Jeong, and S.-W. Son, 2009: Influence of stratospheric quasi-biennial
 507 oscillation on tropical cyclone tracks in the western North Pacific. *Geophysical Research Let-
 508 ters*, **36**, L06 702, doi:10.1029/2009GL037163.

509 Hodges, K., and R. Emerton, 2015: The Prediction of Northern Hemisphere Tropical Cy-
 510 clone Extended Life Cycles by the ECMWF Ensemble and Deterministic Prediction Sys-
 511 tems. Part I: Tropical Cyclone Stage. *Monthly Weather Review*, **143** (12), 5091–5114, doi:
 512 10.1175/MWR-D-13-00385.1.

513 Hodges, K., and P. L. Vidale, 2017: How Well are Tropical Cyclones Represented in Reanalysis
 514 Data Sets? *Journal of Climate*, **submitted**.

- 515 Hodges, K. I., 1994: A General Method for Tracking Analysis and Its Application to Meteorological Data. *Monthly Weather Review*, **122** (11), 2573–2586, doi:http://dx.doi.org/10.1175/1520-0493(1994)122<2573:AGMFTA>2.0.CO;2.
- 518 Hodges, K. I., 1995: Feature Tracking on the Unit Sphere. *Monthly Weather Review*, **123** (12), 3458–2365, doi:http://dx.doi.org/10.1175/1520-0493(1995)123<3458:FTOTUS>2.0.CO;2.
- 520 Hodges, K. I., 1999: Adaptive constraints for feature tracking. *Monthly Weather Review*, **127**, 1362–1373, doi:10.1175/1520-0493(1999)127,1362:ACFFT.2.0.CO;2.
- 522 Huffman, G. J., and D. T. Bolvin, 2012: TRMM and Other Data Precipitation Data Set Documentation. URL ftp://precip.gsfc.nasa.gov/pub/trmmdocs/3B42_3B43_doc.pdf.
- 524 Jiang, H., and E. J. Zipser, 2010: Contribution of Tropical Cyclones to the Global Precipitation from Eight Seasons of TRMM Data: Regional, Seasonal, and Interannual Variations. *Journal of Climate*, **23** (6), 1526–1543, doi:10.1175/2009JCLI3303.1.
- 527 Kim, J.-H., C.-H. Ho, H.-S. Kim, C.-H. Sui, and S. K. Park, 2008: Systematic Variation of Summertime Tropical Cyclone Activity in the Western North Pacific in Relation to the Madden-Julian Oscillation. *Journal of Climate*, **21**, 1171–1191, doi:dx.doi.org/10.1175/2007JCLI1493.1.
- 530 Larson, J., Y. Zhou, and R. W. Higgins, 2005: Characteristics of Landfalling Tropical Cyclones in the United States and Mexico: Climatology and Interannual Variability. *Journal of Climate*, **18** (8), 1247–1262, doi:10.1175/JCLI3317.1.
- 533 Lee, M.-H., C.-H. Ho, J.-H. Kim, and H.-J. Song, 2012: Low-frequency variability of tropical cyclone-induced heavy rainfall over East Asia associated with tropical and North Pacific sea surface temperatures. *Journal of Geophysical Research*, **117**, 12 101, doi:10.1029/2012JD017565.

536 Prat, O. P., and B. R. Nelson, 2013: Mapping the worlds tropical cyclone rainfall contribution
 537 over land using the TRMM Multi-satellite Precipitation Analysis. *Water Resources Research*,
 538 **49**, 7236–7254, doi:10.1002/wrcr.20527.

539 Prat, O. P., and B. R. Nelson, 2016: On the link between tropical cyclones and daily rainfall
 540 extremes derived from global satellite observations. *Journal of Climate*, **in press**, doi:10.1175/
 541 JCLI-D-16-0289.1.

542 Ren, F., G. Wu, W. Dong, X. Wang, Y. Wang, W. Ai, and W. Li, 2006: Changes in tropical
 543 cyclone precipitation over China. *Geophysical Research Letters*, **33 (20)**, L20 702, doi:10.1029/
 544 2006GL027951.

545 Ren Fumin, D. E., Byron Gleason, 2002: Typhoon impacts on chinas precipitation
 546 during 1957-1996. *Advances in Atmospheric Sciences*, **19 (5)**, 943–952, doi:10.1007/%
 547 2Fs00376-002-0057-1.

548 Roberts, M. J., and Coauthors, 2015: Tropical cyclones in the UPSCALE ensemble of
 549 high resolution global climate models. *Journal of Climate*, **28 (2)**, 574–596, doi:10.1175/
 550 JCLI-D-14-00131.1.

551 Serra, Y. L., G. N. Kiladis, and K. I. Hodges, 2010: Tracking and Mean Structure of Easterly
 552 Waves over the Intra-Americas Sea. *Journal of Climate*, **23 (18)**, 4823–4840, doi:10.1175/
 553 2010JCLI3223.1.

554 Song, F., and T. Zhuo, 2014: Interannual Variability of East Asian Summer Monsoon Simulated by
 555 CMIP3 and CMIP5 AGCMs: Skill Dependence on Indian OceanWestern Pacific Anticyclone
 556 Teleconnection. *Journal of Climate*, **27**, 1679–1697, doi:10.1175/JCLI-D-13-00248.1.

557 Sperber, K. R., H. Annamalai, I.-S. Kang, A. Kitoh, A. Moise, A. Turner, B. Wang, and T. Zhou,
 558 2013: The Asian summer monsoon: an intercomparison of CMIP5 vs. CMIP3 simulations of the
 559 late 20th century. *Climate Dynamics*, **41** (9-10), 2711–2744, doi:10.1007/s00382-012-1607-6.

560 Strachan, J., P. L. Vidale, K. Hodges, M. Roberts, and M.-E. Demory, 2013: Investigating global
 561 tropical cyclone activity with a hierarchy of AGCMs: the role of model resolution. *Journal of*
 562 *Climate*, **26** (1), 133–152, doi:10.1175/JCLI-D-12-00012.1.

563 Tian, S.-F., and T. Yasunari, 1998: Climatological aspects and mechanism of spring persistent
 564 rains over central China. *Journal Meteorological Society of Japan*, **76**, 57–71.

565 Villarini, G., and R. F. Denniston, 2015: Contribution of tropical cyclones to extreme rainfall in
 566 Australia. *International Journal of Climatology*, doi:10.1002/joc.4393.

567 Villarini, G., radoslaw Goska, J. a. Smith, and G. a. Vecchi, 2014: North Atlantic Tropical Cyclone
 568 and U.S. Flooding. *Bulletin of the American Meteorological Society*, **95**, 13811388, doi:10.
 569 1175/BAMS-D-13-00060.1.

570 Wang, B., and J. C. Chan, 2002: How Strong ENSO Events Affect Tropical Storm Activity over
 571 the Western North Pacific. *Journal of Climate*, **15**, 1643–1658, doi:http://dx.doi.org/10.1175/
 572 1520-0442(2002)015<1643:HSEEAT>2.0.CO;2.

573 Wang, S.-Y., and T.-C. Chen, 2008: Measuring East Asian Summer Monsoon Rainfall Contribu-
 574 tions by Different Weather Systems over Taiwan. *Journal of Applied Meteorology and Clima-*
 575 *tology*, **47** (7), 2068–2080, doi:10.1175/2007JAMC1821.1.

576 Wu, Y., S. Wu, and P. Zhai, 2007: The impact of tropical cyclones on Hainan Island's extreme and
 577 total precipitation. *International Journal of Climatology*, **27** (8), 1059–1064, doi:10.1002/joc.
 578 1464.

579 Xu, G., T. J. Osborn, and A. J. Matthews, 2016: Moisture transport by Atlantic tropical cyclones
580 onto the North American continent. *Climate Dynamics*, doi:10.1007/s00382-016-3257-6.

LIST OF FIGURES

- Fig. 1.** Monthly counts of westward and northward-moving TCs over the EA ($10^{\circ} - 50^{\circ}\text{N}$, $100^{\circ} - 140^{\circ}\text{E}$) during 1979–2012. TCs are identified from the ERA-Interim reanalysis using the TC feature tracking method. 30
- Fig. 2.** Contribution of TCs to monthly rainfall, calculated using TRMM 3B42 rainfall data for 1998–2012. Units: %. 31
- Fig. 3.** Monthly contributions of TCs to (upper row) extreme rainfall occurrence and (lower row) extreme rainfall amounts, calculated using TRMM 3B42 rainfall data for 1998–2012. Units: %. 32
- Fig. 4.** Monthly accumulated vertically integrated moisture flux divergence for the mean moisture transport ($\nabla \cdot (\bar{\mathbf{v}} \cdot \bar{\mathbf{q}})$, upper panel) and TC eddy moisture transport ($\nabla \cdot (\bar{\mathbf{v}} \cdot \mathbf{q}'_{\text{TC}} + \mathbf{v}'_{\text{TC}} \cdot \bar{\mathbf{q}} + \mathbf{v}'_{\text{TC}} \cdot \mathbf{q}'_{\text{TC}})$, lower panel) (averaged over 1979–2012). Units: mm/month. The dash line in the upper panel indicates the ridge of NWPSH at 500 hPa; Solid lines are geopotential height at 5875 and 5880 m. 33
- Fig. 5.** Seasonal cycle of monthly mean vertically integrated moisture flux passing through the southern (blue) and eastern (red) boundaries. The mean-flow moisture fluxes are shown as solid lines (using the left-hand vertical axis) and TC eddy moisture fluxes as dash lines (using the right-hand vertical axis). The inner panel shows the definition of the southern and eastern boundaries. Positive values indicate moisture is transported into the EA landmass, and negative values indicate moisture is transport out of the EA landmass. Note that the scale of the right-hand vertical axis is an order of magnitude smaller than the left-hand vertical axis. Units: kg/s. 34
- Fig. 6.** Moisture flux (vector) and its divergence (shade) during (a) the westward-moving TC Tai-Kat (2012/08/11 - 2012/08/18) and (b) the northward-moving TC Matsa (2005/08/01 - 2005/08/12). In the text, we only discuss the features with strongest magnitude, which belong the TCs named above. The weaker signals northeast of the Philippines in (a) and east and west of the Philippines in (b) belong to other, weaker TCs which are not discussed in the text. 35
- Fig. 7.** Monthly mean vertically integrated specific humidity during 1979–2012. Units: kg/kg. 36
- Fig. 8.** (Top four panels) Identified TC tracks in each month of JASO during 1979–2012 using the ERA-Interim reanalysis. The two solid black lines show the eastern (21° - 42°N , 121°E) and the southern (21°N , 100° - 121°E) boundaries from Fig. 5; the dotted line is at (16°N , 100° - 121°E). (Bottom panel) The PDF of westward-moving TCs distributing along latitude for each month (Jul–Oct) averaged between 100° – 121°E . A reference line is drawn at 16°N 37

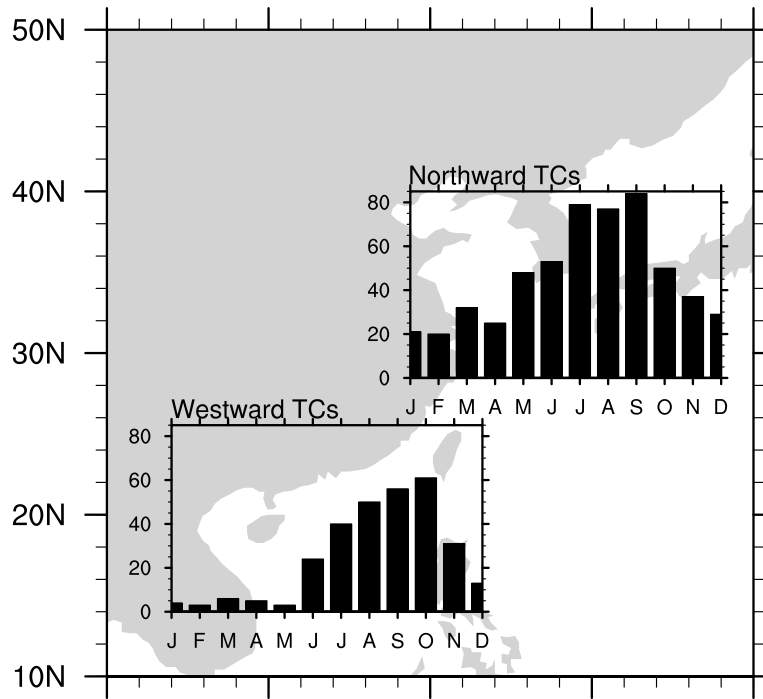


FIG. 1. Monthly counts of westward and northward-moving TCs over the EA ($10^{\circ} - 50^{\circ}\text{N}$, $100^{\circ} - 140^{\circ}\text{E}$) during 1979–2012. TCs are identified from the ERA-Interim reanalysis using the TC feature tracking method.

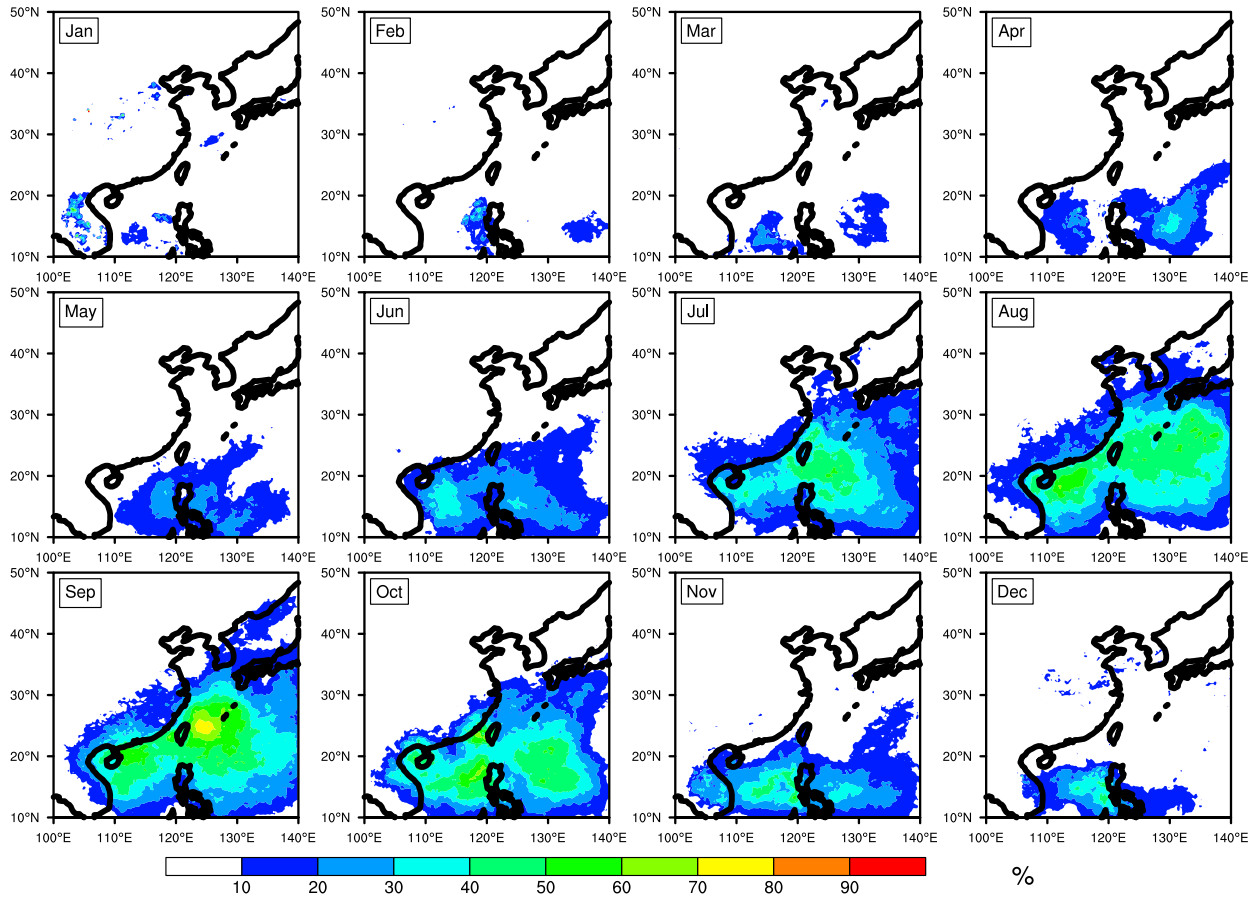


FIG. 2. Contribution of TCs to monthly rainfall, calculated using TRMM 3B42 rainfall data for 1998–2012.
Units: %.

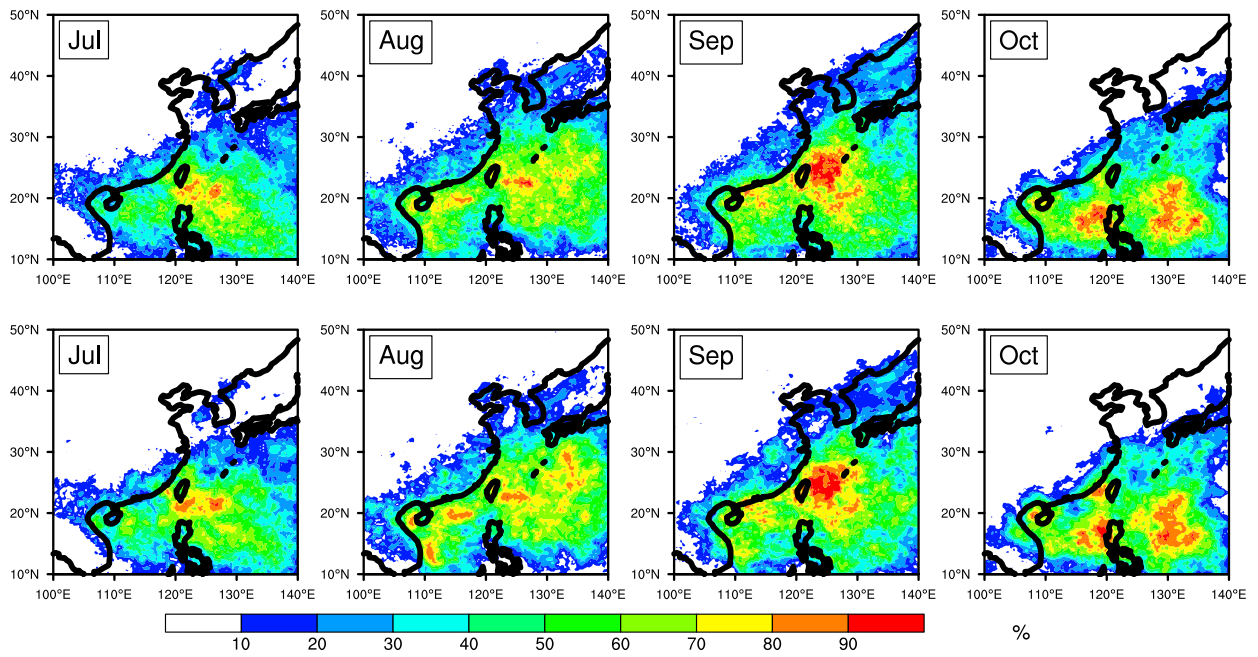
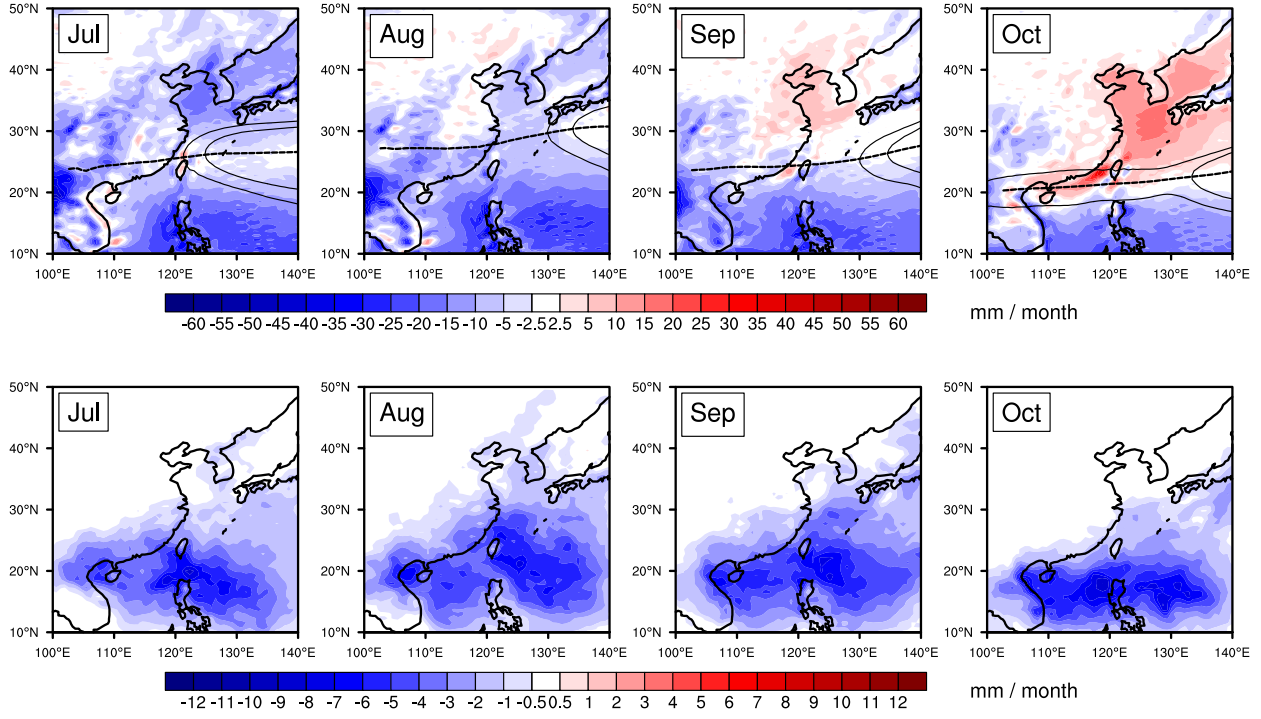


FIG. 3. Monthly contributions of TCs to (upper row) extreme rainfall occurrence and (lower row) extreme
rainfall amounts, calculated using TRMM 3B42 rainfall data for 1998–2012. Units: %.



621 FIG. 4. Monthly accumulated vertically integrated moisture flux divergence for the mean moisture transport
 622 $(\nabla \cdot (\bar{\mathbf{v}} \cdot \bar{\mathbf{q}}))$, upper panel) and TC eddy moisture transport $(\nabla \cdot (\bar{\mathbf{v}} \cdot \mathbf{q}'_{TC} + \mathbf{v}'_{TC} \cdot \bar{\mathbf{q}} + \mathbf{v}'_{TC} \cdot \mathbf{q}'_{TC}))$, lower panel) (averaged
 623 over 1979–2012). Units: mm/month. The dash line in the upper panel indicates the ridge of NWPSH at 500 hPa;
 624 Solid lines are geopotential height at 5875 and 5880 m.

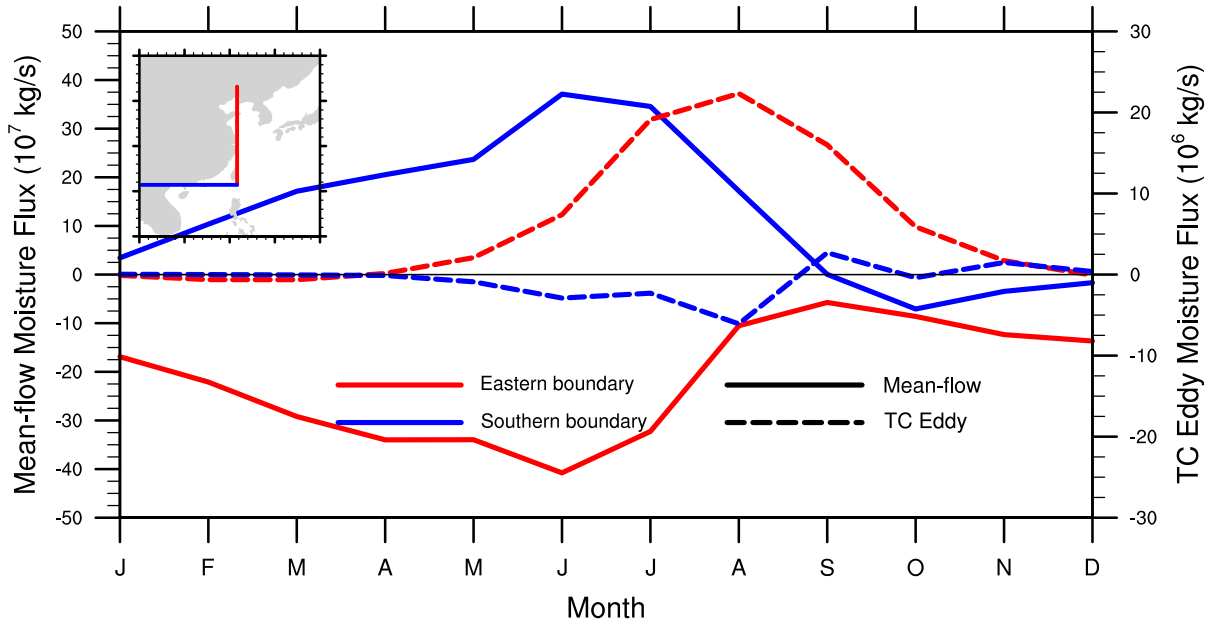


FIG. 5. Seasonal cycle of monthly mean vertically integrated moisture flux passing through the southern (blue) and eastern (red) boundaries. The mean-flow moisture fluxes are shown as solid lines (using the left-hand vertical axis) and TC eddy moisture fluxes as dash lines (using the right-hand vertical axis). The inner panel shows the definition of the southern and eastern boundaries. Positive values indicate moisture is transported into the EA landmass, and negative values indicate moisture is transport out of the EA landmass. Note that the scale of the right-hand vertical axis is an order of magnitude smaller than the left-hand vertical axis. Units: kg/s.

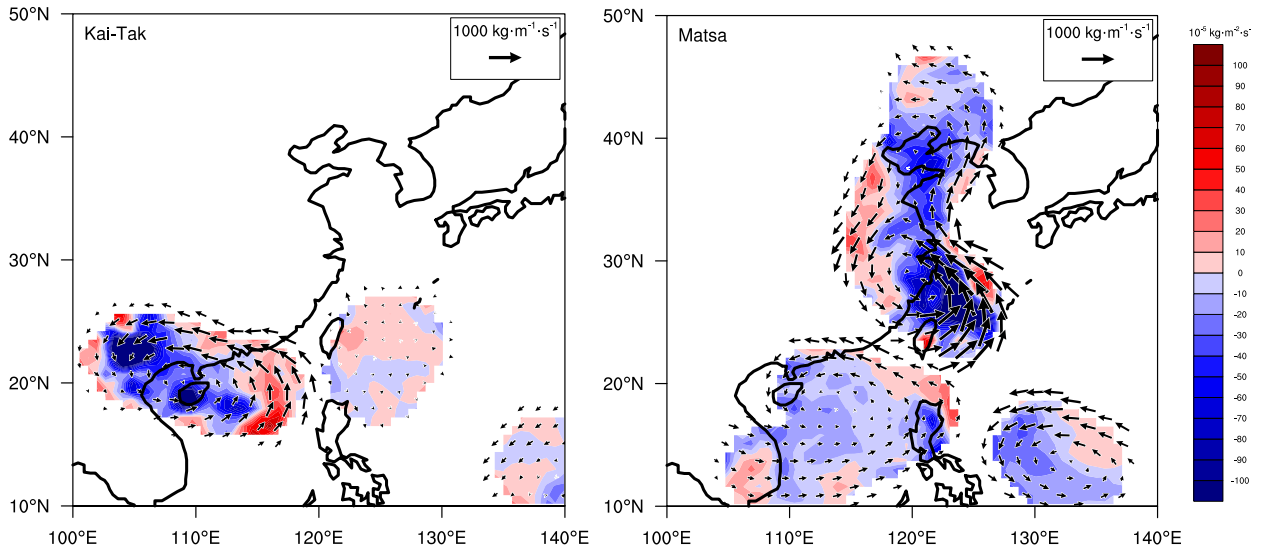


FIG. 6. Moisture flux (vector) and its divergence (shade) during (a) the westward-moving TC Kai-Tak (2012/08/11 - 2012/08/18) and (b) the northward-moving TC Matsa (2005/08/01 - 2005/08/12). In the text, we only discuss the features with strongest magnitude, which belong to the TCs named above. The weaker signals northeast of the Philippines in (a) and east and west of the Philippines in (b) belong to other, weaker TCs which are not discussed in the text.

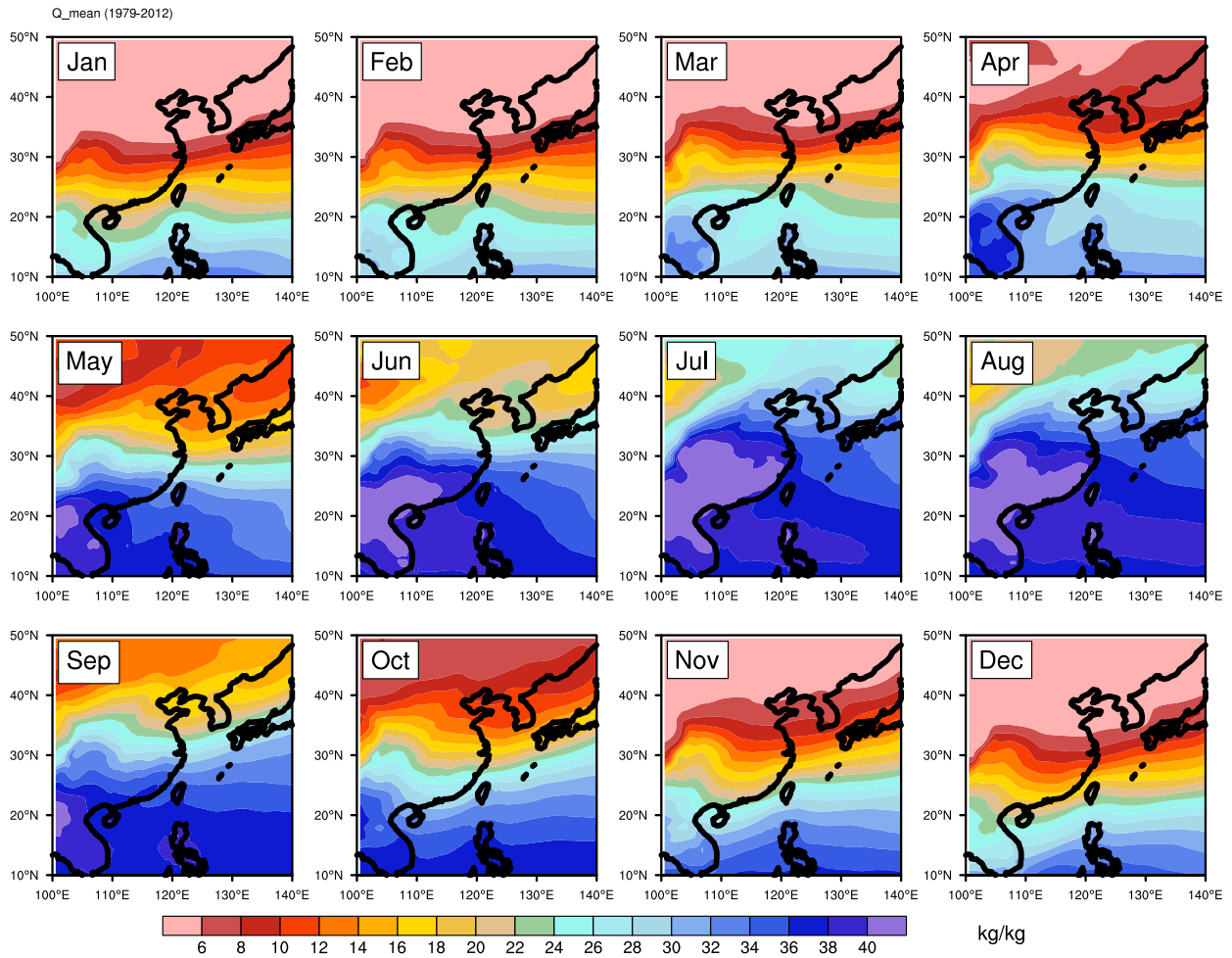


FIG. 7. Monthly mean vertically integrated specific humidity during 1979–2012. Units: kg/kg.

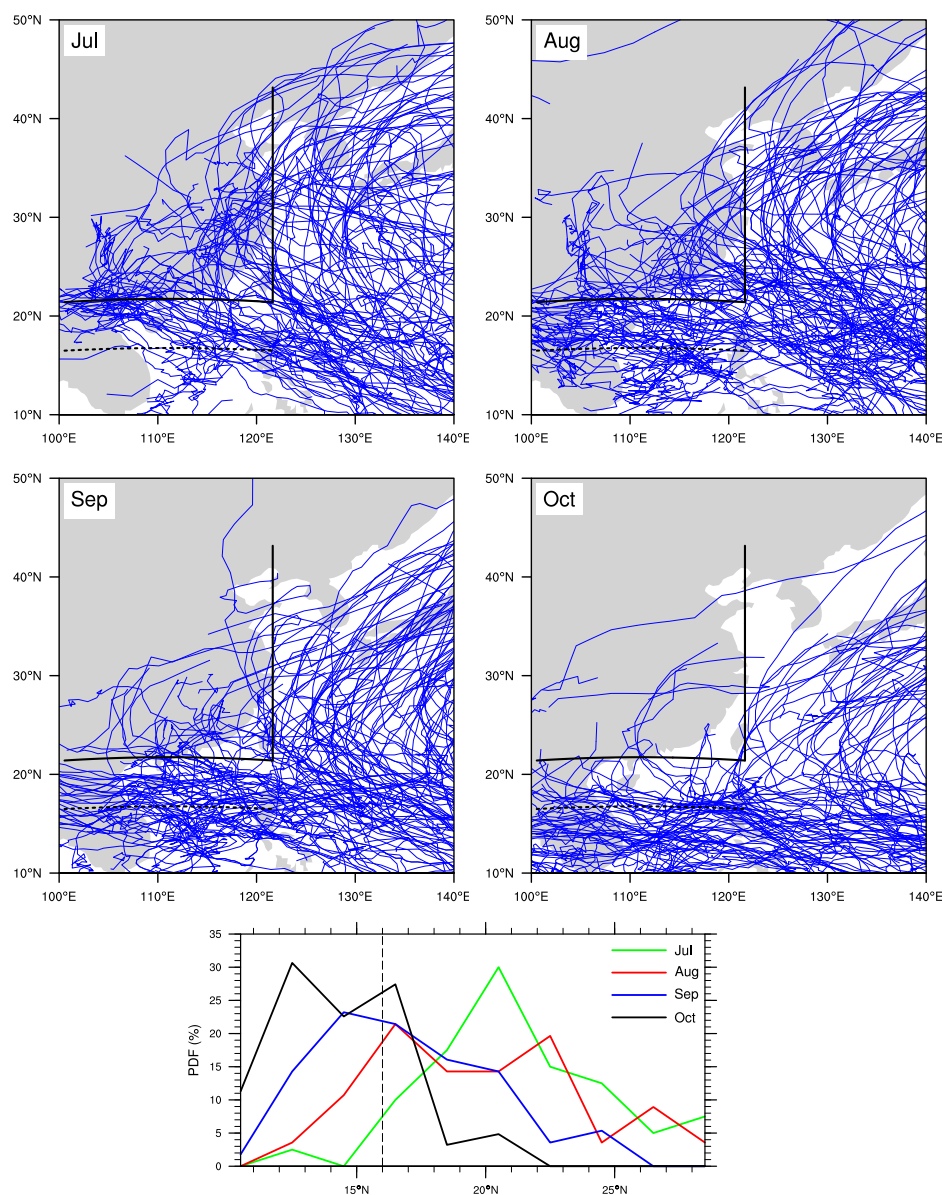


FIG. 8. (Top four panels) Identified TC tracks in each month of JASO during 1979–2012 using the ERA-Interim reanalysis. The two solid black lines show the eastern (21° – 42° N, 121° E) and the southern (21° N, 100° – 121° E) boundaries from Fig. 5; the dotted line is at (16° N, 100° – 121° E). (Bottom panel) The PDF of westward-moving TCs distributing along latitude for each month (Jul–Oct) averaged between 100° – 121° E. A reference line is drawn at 16° N.